*Geophysical Journal* (1988) **95**, 421–432

# Magnetic properties of synthetic analogues of the altered olivines of igneous rocks

D. Brewster and W. O'Reilly

*Department of Geophysics & Planetary Physics, School of Physics, The University of Newcastle upon Tyne, Newcastle upon Tyne NE1 7RU, UK*

Accepted 1988 June 8. Received 1988 June 8; in original form 1988 March 11



## SUMMARY

A laboratory simulation has been made of the high temperature deuteric alteration of olivine such as occurs in slowly cooled basic intrusions. Three compositions in the Forsterite/Fayalite solid solution series were synthesized by a three-firing method using self buffering and controlled atmosphere to obtain material containing no detectable magnetite ($Fe_3O_4$) as a contaminant (<0.005 per cent).

The prepared olivines were oxidized between 850 and 1280 °C at oxygen fugacities of between $10^{-13.1}$ and $10^{-5.7}$ atmospheres. The composition and concentration of the multiphase oxidation products were studied by magnetic, optical, electron optical and X-ray methods. The magnetic constituent of the intergrowth was magnetite. Below about 1150 °C the microstructure is similar to the 'dendritic' intergrowths found, for example, in the altered olivine of the Central Layered Intrusion of the Isle of Rhum. Above about 1150 °C the form may be similar to 'symplectite' intergrowths.

The magnetization process parameters (coercive force, etc.) vary systematically with temperature of oxidation ($T_{ox}$) which evidently controls the microstructure of the magnetite. The magnetite produced is magnetically 'hard', samples altered at 900 °C and 950 °C having higher coercive force ($H_c$) than any magnetite reported in the literature. The room temperature properties appear to bridge the published trends found in 'grown crystal' magnetites and 'crushed grains'. Inferred *effective* grain sizes of the complex intergrowths range from 0.1 to 3 $\mu$m as $T_{ox}$ increases from 900 to 1200 °C. The temperature dependence of magnetization process parameters (principally $H_c$) measured between room temperature and the Curie point are modelled in terms of (i) monodomain grains subject to thermal fluctuations, (ii) monodomain grains not subject to thermal fluctuations, and (iii) as multidomain grains. Model (i) yields plausible values for effective grain dimensions and length/diameter ratios, higher $T_{ox}$ producing larger, more equidimensional particles. Model (ii) suggests that the relative importance of cubic and uniaxial anisotropies may be influenced by a microstructure-dependent uniaxial particle–particle interaction term. Model (iii) implies that, if domain walls are pinned by both surface and volume defects, magnetostriction plays a greater role in volume pinning than in surface pinning. Plausible values of demagnetizing factors appropriate to grains with few domains are produced by model (iii).

**Key words:** Olivines, oxidation, magnetite, magnetization process

## 1 INTRODUCTION

The iron-bearing silicate minerals may alter to produce inclusions of iron oxides. In a recent example, Brearley & Champness (1986) report the presence of magnetite particles in alamandine-rich metamorphic garnets in gneiss, hornfels and schists. Magnetite rods in the plagioclase of ocean floor gabbros are described by Davis (1981). The origin of the dendritic magnetite inclusions in the olivines of the ultrabasic layered intrusion of the Isle of Rhum, Scotland, has been discussed by Putnis (1979).

The potential of the iron oxide alteration products as carriers of components of the natural remanent magnetization (NRM) of the host rocks has been long recognized (e.g. Evans, McElhinny & Gifford 1968; Hargraves & Young 1969; Morgan & Smith 1981). When the alteration process occurs at high temperature (above the Curie points of magnetite and haematite), the thermoremanence (TRM) acquired by the iron oxides in fine particle form can be a stable record of the palaeomagnetic field at a determinable time. When the alteration occurs during metamorphism, or low temperature alteration, the remanence may be a

mixture of chemical remanence (CRM) and partial thermoremanence (PTRM), e.g. in the 'serpentinization' or 'iddingsitization' of olivines.

The experimental studies which have been made to elucidate the mechanism by which silicates alter, have concentrated on the oxidation of olivines in air. Haggerty & Baker (1967) and Champness & Gay (1968) oxidized olivines in air at temperatures between 500 and 1000 °C. The ultimate oxide oxidation phase was haematite with an intermediate spinel phase, the latter being near to magnetite in composition, at least for oxidation temperatures above 900 °C. Riding (1969) found the intensity of TRM of air-oxidized olivines high enough to account for the observed NRMs of olivine-bearing rocks. The low temperature oxidation of synthetic olivines in air or pure oxygen to produce magnetite below the Curie point temperature, and the acquisition of CRM, TRM and anhysteretic remanence by the produced magnetite, has been described by Hoye & O'Reilly (1973) and Hoye & Evans (1975). Intense and stable remanences were obtained. Hoffmann & Soffel (1986) report the production of Mg–Fe spinels by oxidation of a range of synthetic Mg–Fe olivines below 600 °C. Above 700 °C magnetite was produced.

The purpose of the present investigation is to more closely simulate the high temperature deuteric oxidation of olivines which takes place while cooling in the atmosphere within the igneous body. The oxidation experiments are therefore to be carried out at temperatures up to about 1250 °C, not in air, but in a controlled atmosphere so that magnetite may be produced. The products of deuteric oxidation in nature may be good candidates to carry an unequivocal record of the geomagnetic field. The magnetic characteristics of such magnetite are therefore of considerable interest to any palaeomagnetic application of olivine-bearing rocks. The magnetite of the 'dendritic' and 'symplectite' intergrowths of the deuterically oxidized olivines has a more complex microstructure than the materials which provide the bulk of the magnetite data to be found in the literature. The available magnetite data may therefore be a poor guide to the expected magnetic properties of the oxidized olivines in nature. At the same time the synthetic analogues of the complex naturally occurring material provide problems of physical interest in the attempt to match their observed properties to models for the magnetization process.

## 2 PREPARATION OF THE INTERGROWN MATERIAL

### 2.1 Synthesis of the olivines

The starting ingredients were: Fe, Johnson Matthey Chemicals (JMC) grade 2; $Fe_2O_3$, JMC 'Puratronic' grade 2; $SiO_2$, Thermal Syndicate 'Spectrasil' synthetic silica, total magnetic impurities <0.2 ppm; MgO, JMC 'Puratronic' grade 2.

A three-stage firing process was adopted. Stoichiometric mixtures of Fe, $Fe_2O_3$, $SiO_2$ and MgO were thoroughly mixed in a mechanical shaker before being pressed into pellets 6 mm long and 6 mm in diameter under a pressure of about 2 GPa. The pellets were sealed in quartz tubes evacuated to about 1 mPa, heated at 1000 °C for 24 hr and air-quenched to room temperature. The pellets were pulverized under acetone, dried, repressed into pellets which were encapsulated, and fired a second time at 1000 °C for 24 hr. The material was again pulverized and repelleted for the final 24 hr firing under a controlled atmosphere appropriate to olivine at the firing temperature. Using the data of Nitsan (1974), an oxygen fugacity of $10^{-11.6}$ atmospheres provided by a flowing $CO$–$CO_2$ mixture was adopted for the firing temperature of 1120 °C. At the end of the third 24 hr firing period, the sample was quenched into a water cooled section at one end of the furnace while remaining in the controlled atmosphere. The sample temperature fell to about 100 °C in approximately 1 min. After each of the three stages of the procedure, the material produced was investigated by optical, X-ray, electron optical and magnetic methods.

Fragments of pellet were embedded in cold mounting resin, polished and observed under reflected light (up to ×1325 with oil immersion). Within the yellowish matrix many small bright opaque grains could be seen after the first firing. These were considerably reduced in number after the second firing and were undetectable after the third. The thrice-fired material was analysed using the electron microprobe. The material appeared uniform in electron and X-ray images, and the olivine compositions calculated from the element concentrations (oxygen determined by difference) are in good agreement with the target values (Table 1). This is, of course, only a measure of the accuracy achieved in weighing out the ingredients if the length scale of any compositional microstructure is well below the electron beam diameter. We code the compositions of the $(Fe_xMg_{1-x})_2\,SiO_4$ $(0 < x < 1)$ series as FA100$x$, i.e. FA50 has 50 per cent Fayalite.

Crushed specimens were investigated by the X-ray powder method using a Debye–Scherrer camera and Fe radiation. After the second firing, in addition to the olivine lines, two lines at 2.89 and 3.17 Å could be attributed to enstatite ($MgSiO_3$). After the third firing, only olivine lines were visible on the film. This limits the concentration of a single second, non-olivine, phase to a maximum of about 2 per cent. The high-angle back reflections are most sensitive to composition variation, and the line indexed as (452, 116) was used to compare the compositions of the present samples to the compositions of the suite prepared by Hoye & O'Reilly (1972). The inferred compositions of the samples of the present investigation are listed in Table 1.

Magnetization curves run at room temperature on a vibrating sample magnetometer (VSM) showed the presence of a ferromagnetic phase, together with the silicate, after the first two firings. After the third firing the magnetization-field curve is a straight diagonal line through the origin consistent

**Table 1.** Analysis for the composition of the synthesized Fe–Mg olivines by electron microprobe and the X-ray powder method. The room temperature magnetic susceptibility is also given.

| Target FA100$x$ | Composition EPMA (±0.5) | Composition $d$(452, 116) (±0.5) | Room temperature susceptibility ($10^{-8}$ m$^3$ kg$^{-1}$) (±3) |
|---|---|---|---|
| $x = 0.3$, FA30 | 30.2 | 31.1 | 51 |
| $x = 0.5$, FA50 | 49.4 | 48.3 | 73 |
| $x = 0.75$, FA75 | 75.9 | 74.2 | 111 |

with the target olivine (an antiferromagnet above the Néel temperature). The contribution of a ferromagnetic contaminant is below the noise level of the instrument. This imposes an upper limit to magnetite ($Fe_3O_4$) concentration of 0.005 per cent. The room temperature magnetic susceptibility (Table 1) of the thrice-fired material is in good agreement with data obtained by Hoye & O'Reilly (1972) and Hoffmann & Soffel (1986).

### 2.2 Oxidation of the olivines

The conditions for oxidation were chosen with reference to the oxygen fugacity-temperature curves appropriate to the stability of the olivine (Nitsan 1974) and to equilibrium between magnetite and haematite (e.g. Lindsley 1976). In the zone between the two curves the magnetic product of simulated deuteric oxidation will be magnetite only. Oxidation temperatures were chosen between 850 and 1280 °C and oxygen fugacities between $10^{-13.1}$ and $10^{-5.7}$ atmospheres. The lower temperature was imposed by limitations in the controlled atmosphere system. It proved impracticable to control the very low concentrations of CO to achieve the required oxygen fugacity below this lower temperature (about 850 °C for FA75, 850 °C for FA50 and 1000 °C for FA30). The upper limiting temperature was imposed by the need to avoid melting the olivine and the unavoidable destruction of the alumina boat in which the pellets were placed during oxidation, and the likely contamination of the silicate sample by the boat. The oxidizing conditions were maintained for 24 hr and the sample quenched. The degree and nature of the oxidation achieved was determined by optical, X-ray, electron optical and magnetic methods.

From the comprehensive determination of magnetic properties (saturation magnetization, susceptibility, etc.) at elevated temperatures (Section 3.3) it appears that the magnetic phase present in the oxidized olivines is magnetite with Curie point at 570–580 °C. Magnesium content in the oxide must be less than about 0.1 per cent. Having established the composition of the magnetic phase, the concentration can be deduced from the saturation magnetization of the oxidized intergrowth. This was measured using a vibrating sample magnetometer (VSM). Assuming all the $Fe^{3+}$ is contained in the magnetite, the oxidation reaction can be expressed:

$$(Fe_xMg_{1-x})_2SiO_4 + (2/3)xzO \rightarrow [2x(1-z)FeO.2(1-x)MgO.SiO_2] + (2/3)xzFe_3O_4,$$

(silicate phases)

where $z$ is the fraction of reaction or oxidation parameter, which will take values from 0 to 1. When $p$ is the weight per cent of $Fe_3O_4$ determined from the saturation magnetization of the intergrown oxidation product, then

$$z = p.(1.40 + 0.64x)/(154x).$$

For FA30, $z$ values were obtained up to about 0.7 ($Fe_3O_4$ concentration 20 per cent); for FA50 up to about 0.5 (25 per cent), and up to 0.3 (18 per cent) for FA75.

The changing bulk composition of the silicate phases during oxidation can be plotted on the MgO–$SiO_2$–FeO ternary diagram (Fig. 1). The compositions follow lines running upwards and to the left (increasing $SiO_2$ and MgO concentrations). The silicate products of oxidizing FA30 and FA50 have penetrated the region in which the stable phases are co-existing olivine and pyroxene (Bowen & Schairer 1935). The products of the oxidation of FA75 first pass through a region in which olivine and $SiO_2$ co-exist, then traverse a narrow field in which olivine, pyroxene and $SiO_2$ are stable before entering the olvine/pyroxene field.

X-ray analysis of the oxidized material showed that all

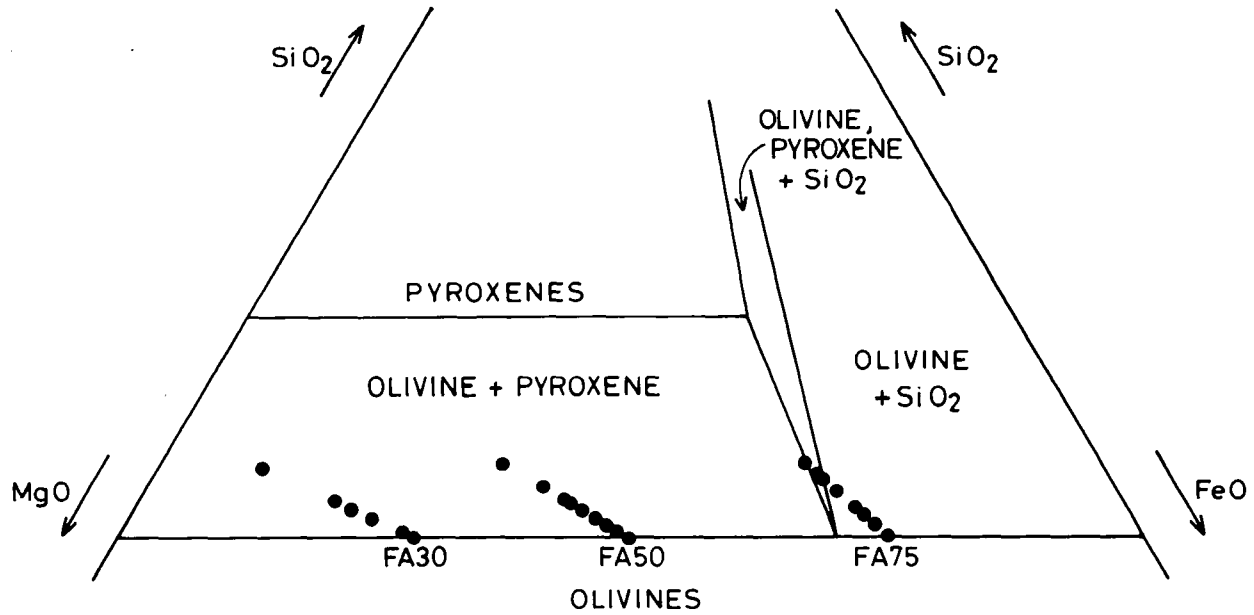


**Figure 1.** A section of the MgO–$SiO_2$–FeO ternary phase diagram (Bowen & Schairer 1935). The indicated tracks show the bulk composition of the silicate phases which accompany the progressive production of magnetite during oxidation of the olivines FA30, FA50 and FA75. The points on the tracks are the compositions achieved in the present study in which oxidation took place at temperatures from 850 to 1280 °C under a controlled CO–$CO_2$ atmosphere.

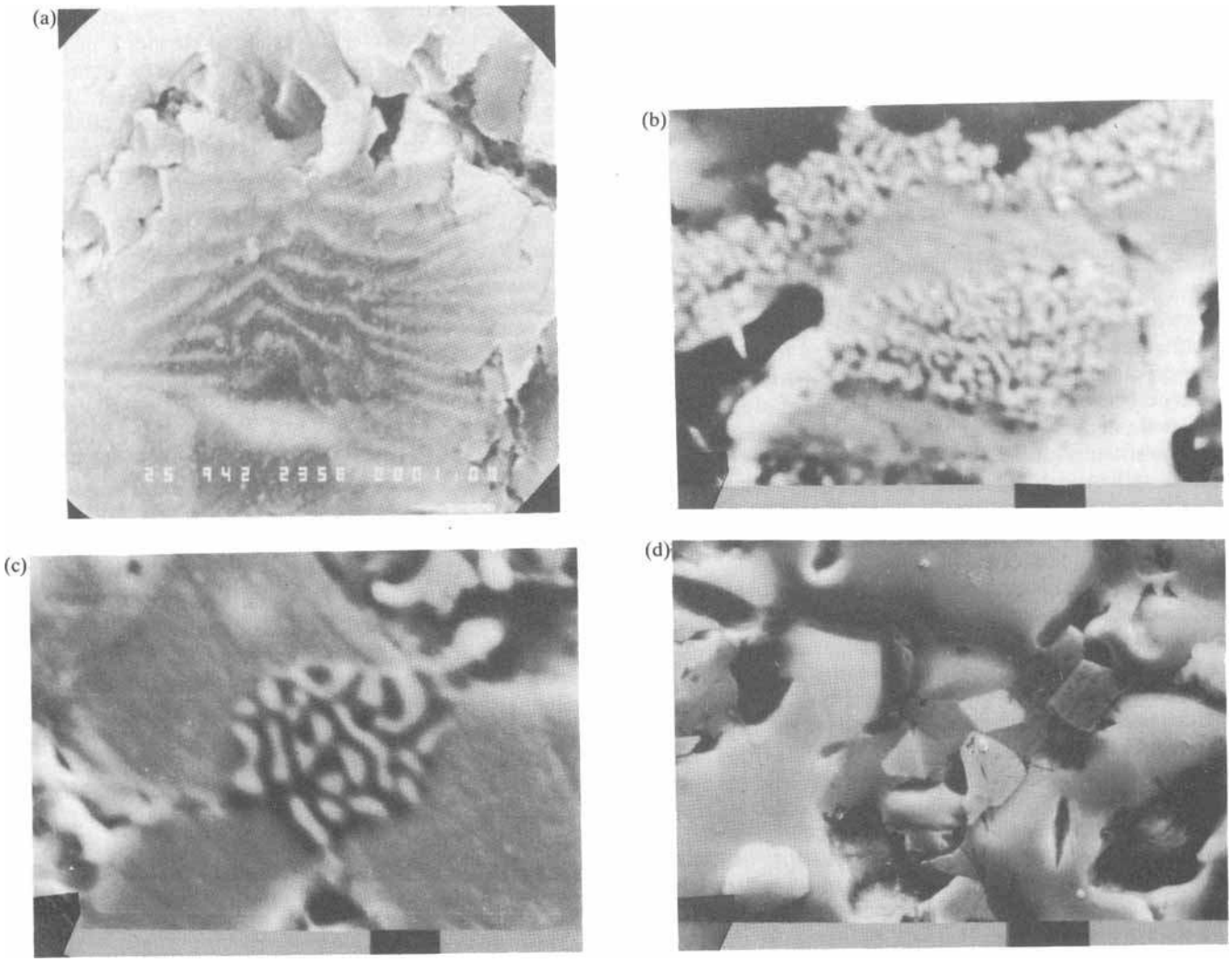


**Plate 1.** Some representative electron micrographs of the oxidized olivines. Plates (a), (b) and (c) are similar to the 'dendritic' intergrowths found in nature in which the magnetite occurs as clusters of lamellae intergrown with silicate. In Plate (a) the FA50 has been oxidized at 1060 °C, the scale bar is 1 $\mu$m and the slim, elongated pale magnetite lamellae are separated by a darker pyroxene. In Plate (b) FA75 has been oxidized at 1060 °C, the scale bar is 2 $\mu$m. The dendritic zones are spread across the upper part of the plate and near the centre. The thick bright magnetite lamellae are separated by dark cristobalite. The grey areas between the dendritic zones are olivine poorer in iron than FA75. Plate (c) shows FA75 oxidized at 1120 °C and the scale bar is 2 $\mu$m. The dendritic intergrowth in the centre of the plate contains fewer and larger regions of the two phases (magnetite and crystobalite) than Plate (b). Again the surrounding grey area is olivine. Plate (d) (FA75 at 1200 °C; scale bar: 10 $\mu$m) is similar to 'symplectite' intergrowths of magnetite and silicate. Pale euhedral magnetite grains can be seen near the centre of the plate surrounded by darker grey cristobalite. The extended pale grey regions are olivine.

samples contained olivine with an inferred lower Fe concentration than the starting material, and a spinel phase (the magnetite revealed by magnetic measurement). In the more highly oxidized samples of FA30 and FA50, pyroxene was also detected. In the less oxidized samples, the second silicate phase is assumed to be present but below the limit of detection. In some samples, depending presumably upon the oxidation temperature and the initial olivine Fe–Mg ratio, clinopyroxene was formed, in others orthopyroxene. Distinction between the two forms was made difficult because of the coincidence of several lines of the pyroxenes with those of olivine and magnetite. No detectable quantity of pyroxene was discovered in the more highly oxidized FA75, the second silicate phase being cristobalite ($SiO_2$) as expected from the phase diagram (Fig. 1).

The size and shape of the magnetite grains, and the relationship of the grains to each other and to the silicate host, was investigated using electron microscopy. It was found that the temperature of oxidation played the major role in determining the microstructure. At oxidizing temperatures of 1200 and 1280 °C well-formed distinct magnetite grains of typical length 5 $\mu$m were visible, set in a matrix darker in colour than the surrounding olivine. For samples oxidized at lower temperatures (1060 and 1120 °C) the magnetite was found to have developed as localized groups of lamellae intergrown with, again, a mineral darker in colour than the olivine. At lower oxidation temperatures (850, 900, 950 and 1000 °C) the scale of any intergrowths

was too small to be resolved by the electron microscope. For the samples oxidized at 1120 °C and above, the composition of the dark phase surrounding or intergrown with the magnetite was determined by Energy Dispersive X-ray Analysis. The X-ray diffraction results were thus confirmed, the analyses of the FA30 and FA50 samples being consistent with pyroxene and the FA75 with cristobalite. Some representative micrographs are shown in Plate 1.

### 2.3 Discussion of the oxidation process

The mechanism by which iron oxides are produced by oxidation of naturally occurring olivines has been discussed by Haggerty & Baker (1967), Champness & Gay (1968) and more recently by Putnis (1979). The products obtained at 1200 and 1280 °C in the present investigation may be similar to what have been described as 'symplectite' intergrowths. These are believed to result from the direct formation of magnetite and pyroxene (cristobalite in our more Fe-rich synthetic olivines) initiated at nucleation points. A precursor phase may not be needed in the production of such symplectite intergrowths if temperature is high enough to provide the energy required for nucleation. The products obtained at 1060 and 1120 °C (and presumably at lower temperatures) may be similar to the 'dendritic' intergrowths exemplified by olivines of the Rhum layered intrusion which are discussed by Putnis (1979). A metastable intermediate oxidized cation-deficient olivine phase is postulated in the early stages of oxidation at temperatures low enough that the probability of direct nucleation to the equilibrium phases is very small. Only a limited degree of non-stoichiometry of the olivine is possible before the intermediate phase suffers 'eutectoidal' decomposition by a 'pearlitic' precipitation mechanism. The envelope of the intergrown cluster of magnetite lamellae is a relic of the local extent of the precursor phase.

## 3 MAGNETIC MEASUREMENTS

### 3.1 Preparation of samples

Cubes of approximately 3 mm side were cut from the cylindrical pellets using a diamond saw and shaped roughly into spheres using a rotating abrasive disk. Each near-spherical sample was milled for several hours by being driven by compressed air around a 10 cm diameter race track with abrasive sides. The resultant 2 mm diameter sphere was packed into a quartz tube using quartz wool and sealed off under vacuum.

### 3.2 Room temperature measurements

Hysteresis loops which yielded coercive force ($H_c$), saturation magnetization ($M_s$) and saturation remanence ($M_{rs}$) were measured on the VSM and initial susceptibility ($\chi$) on a bridge. Coercive force of remanence ($H_{cr}$) was measured using a DC demagnetizing coil and spinner magnetometer.

As expected from the electron optical observations which had revealed a dependence of microstructure on temperature of oxidation ($T_{ox}$), the magnetization process parameters show a strong systematic $T_{ox}$ dependence. $M_{rs}/M_s$ values range from 0.02 to 0.4, $H_c$ from about 2 to about 40 $kAm^{-1}$ and $\chi$ from about 2 to about 5 (per unit volume specific to inferred magnetite content). The effect of oxygen fugacity was relatively small and unsystematic, e.g. the $H_c$ values of a suite of five FA50 samples oxidized at 1120 °C and at fugacities between $10^{-8.3}$ and $10^{-7.8}$ atmospheres were scattered by only ±20 per cent around a mean value of 6 $kAm^{-1}$. Accordingly, the data are displayed in Fig. 2(a–d) with $T_{ox}$ as the independent variable.

It can be seen that the greater part of the variation in $H_c$ and $M_{rs}/M_s$ takes place in the range of production of dendritic intergrowths (1120 °C and below). Within this range, the complex microstructure might seem to be inexpressible in a single parameter (such as the 'grain size') describing the shapes, volumes and inter-relations of the components of an intergrowth. Nevertheless the uniform variation of the magnetization process parameters suggests that such a single microstructural variable exists and is here finding expression in $T_{ox}$. A preliminary survey of the data suggests that an 'effective grain volume' is decreasing as $T_{ox}$ decreases, that a state closely approximating to the stable monodomain state is reached, and that at the lowest $T_{ox}$ the effective volume may be entering the superparamagnetic regime.

The $H_{cr}/H_c$ variation contrasts markedly with the $H_c$ and $M_{rs}/M_s$ behaviour in that the variation within the dendritic intergrowth region is less pronounced compared with that which takes place on entering the symplectite region. Within the dendritic region the $H_{cr}/H_c$ values are characteristic of grains with few domains, the lowest value (1.2) approaching the model value for non-interacting uniaxial monodomain grains (1.1).

### 3.3 The magnetization process at elevated temperature

The inference concerning the decreasing effective volume, or other systematic microstructural variation with decreasing $T_{ox}$, is also borne out by the observed temperature dependence of magnetization process parameters.

The temperature dependence of initial susceptibility for members of the FA75 suite shown in Fig. 3 exhibits a progressively more enhanced Hopkinson peak as $T_{ox}$ is reduced. The coercive force of members of the FA75 suite falls more rapidly with ascending temperature (Fig. 4) as $T_{ox}$ is reduced, as also does the ratio $M_{rs}/M_s$ (Fig. 5).

## 4 DISCUSSION OF THE MAGNETIC MEASUREMENTS

### 4.1 The room temperature data

Some measure of an 'effective grain size' of the intergrown magnetite may be obtained by comparing the room-temperature magnetization process parameters with those obtained in other investigations on natural and synthetic magnetite grains of measured grain size. In a recent review, Dunlop (1986) has distinguished between 'grown crystals' and 'particles produced by crushing'. The former tend to be small particles (<0.5 μm) and are two to five times 'softer' than would be expected from the extrapolation of the data of the crushed grains (1–200 μm) down into the

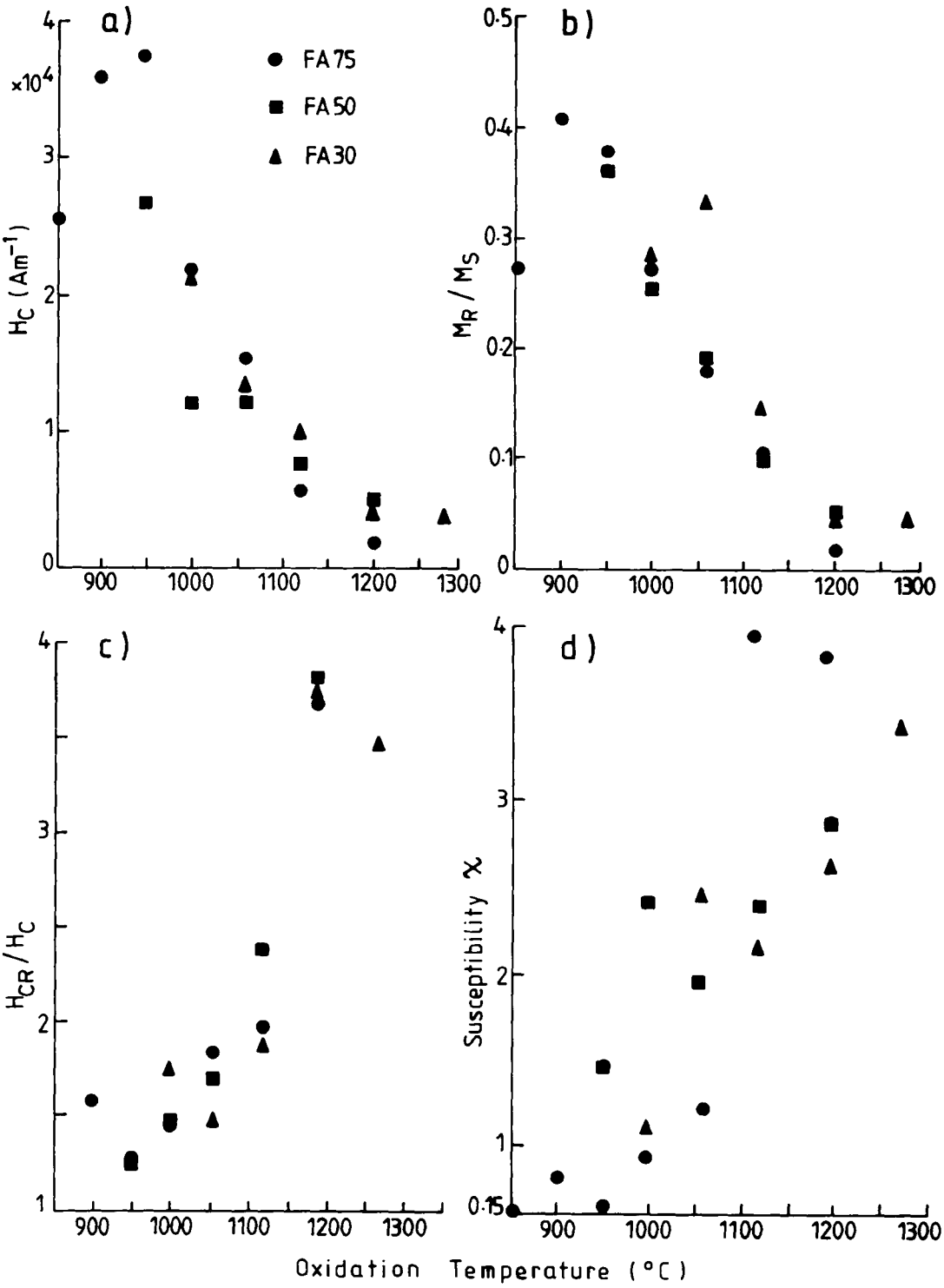


**Figure 2.** Magnetization process parameters of the altered olivines, measured at room temperature, plotted against the temperature of oxidation ($T_{ox}$) as the independent variable. (a) The coercive force ($H_c$); (b) The ratio of saturation remanence to saturation magnetization ($M_{rs}/M_s$); (c) The ratio of coercive force of remanence ($H_{cr}$) to $H_c$; (d) The initial susceptibility ($\chi$) (specific to the inferred $Fe_3O_4$ concentration). Despite the complexity of the microstructure in these laboratory analogues of dendritic intergrowths, the data suggest the systematic variation of a single microstructural parameter here finding expression as $T_{ox}$.

sub-micrometre region. The magnetite of the present investigation has not been prepared by crushing larger grains so might seem to qualify as 'grown crystals'. It is, however, much harder than any grown crystal data, indeed the FA75 oxidized at 900 and 950 °C have higher $H_c$ than any of the published magnetite data whether grown or crushed. On the other hand the FA75 oxidized at 1200 °C has a low $H_c$ similar to crushed grains of sizes 50–100 $\mu$m, very much larger than the few micrometres revealed by the electron microscope. The magnetite in the $T_{ox} = 1060$ and 1120 °C samples is intergrown with cristobalite (in the FA75 series) and it is reasonable to suppose this also to be true in

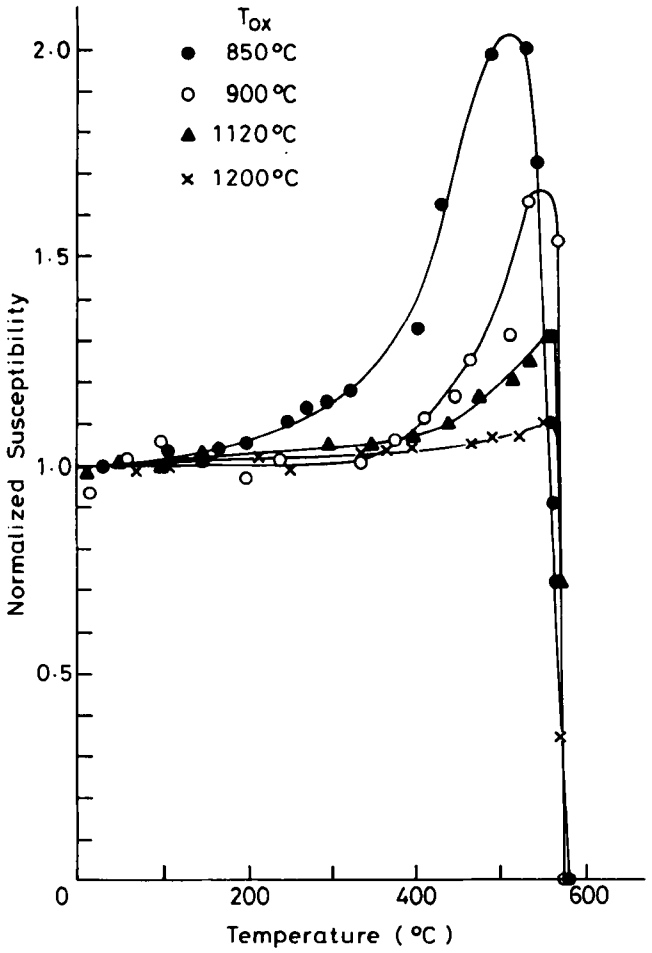


**Figure 3.** The temperature dependence of the normalized initial susceptibility of the FA75 suite with oxidation temperature $T_{ox}$ as a parameter. The Hopkinson peak is progressively more pronounced as $T_{ox}$ decreases.

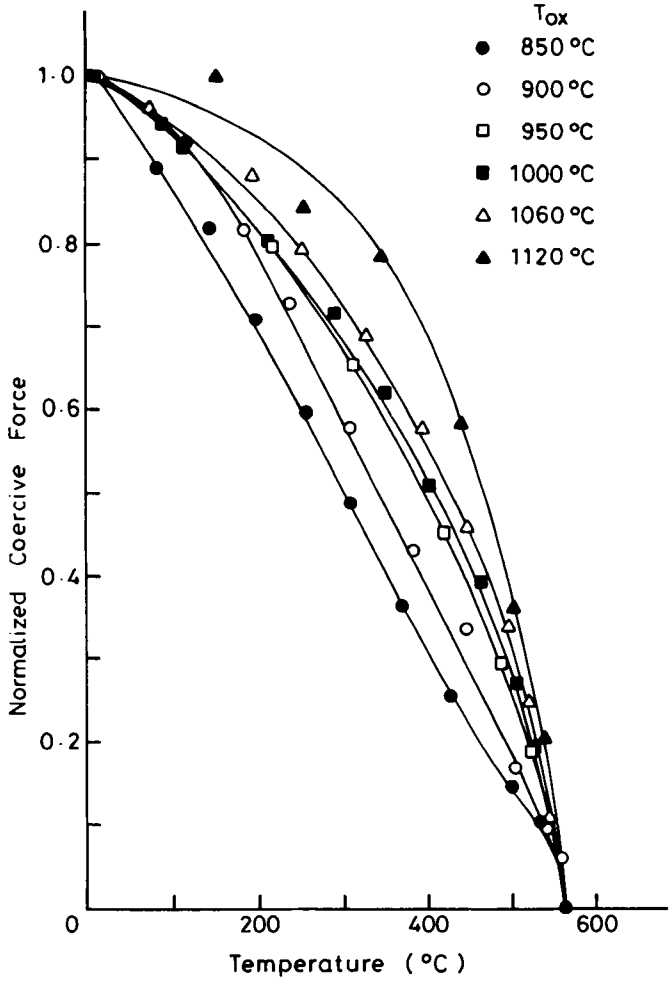


**Figure 4.** The temperature dependence of the normalized coercive force of the FA75 suite with oxidation temperature $T_{ox}$ as a parameter. The fall in $H_c$ with ascending temperature is progressively more rapid as $T_{ox}$ decreases.

the lower $T_{ox}$ samples. The lattice mis-match between the iron and silicon oxides, and the large area of surface at the interface between the two phases, is no doubt the source of the strain which makes these grown crystals behave more like crushed grains. As the dendritic microstructure gives way to the symplectite structure and the magnetite grain volumes increase also, the role of the interface will become less dominant. The $H_c$ of the $T_{ox} = 1200\,°C$ sample could readily be ascribed to a grown crystal of size 2–5 $\mu$m on the basis of an upward extrapolation of the grown crystal collected data of Dunlop (1986). The present data may be accommodated by taking a hypothetical linear trend on the $\log(H_c) - \log(d)$ of Dunlop's (1986) compilation (Fig. 5 of that paper) spanning the grown crystal and crushed grain trends. If $T_{ox} = 1200\,°C$ lies on the grown crystal trend and $T_{ox} = 900\,°C$ lies midway between the annealed and unannealed crushed grain trend, then the inferred *effective* grain sizes of the FA75 suite based on measured $H_c$ are 0.1, 0.2, 0.3, 0.8 and 3 $\mu$m as $T_{ox}$ ascends from 900 to 1200 °C. The $T_{ox} = 850\,°C$ is not included on the hypothetical trend (on which it would have a grain size 0.1–0.2 $\mu$m). Perhaps the measured $H_c$ has been reduced by thermal agitation at room temperature, assisted by the interaction fields within the intergrowths.

### 4.2 The high temperature data

The temperature dependence of the magnetization process also varies throughout the oxidized suite with microstructure presumed to be the independent parameter, given that the composition of the magnetic component is the same in all members of the suite. The temperature dependence of the magnetization process parameters comes from the dependence on thermal energy $kT$, and the temperature dependence of the intrinsic material properties $M_s(T)$, $K(T)$ and $\lambda(T)$—the spontaneous magnetization, the crystal anisotropy constant and the magnetostriction coefficient. The material properties combine with the microstructure—the size and shape of the grains, including internal voids, the relationship between the magnetic crystal and neighbouring material—to control the barriers to magnetization change and the domain state. For a temperature independent microstructure, the height of the barriers and the number of domains change as $M_s$, $K$ and $\lambda$ change via $T$. In the well-behaved zone approaching the Curie point a power law dependence on $M_s$ is often taken to be a good analytical approximation of the temperature dependence of $K$ and $\lambda$, e.g. $K \sim M_s^8(T)$ (Fletcher & O'Reilly 1974), $\lambda \sim M_s^2(T)$

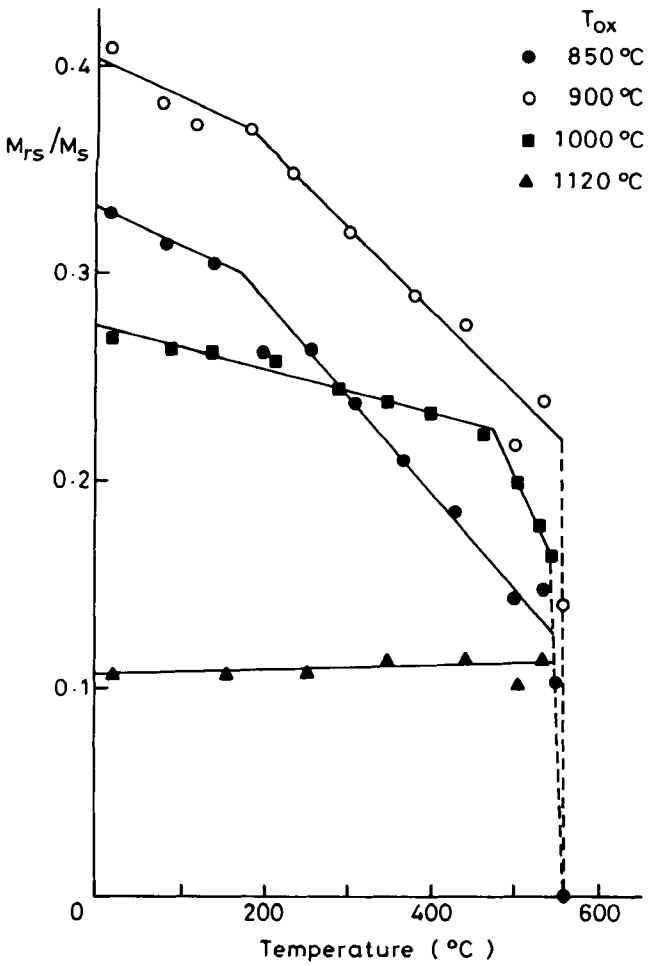


**Figure 5.** The temperature dependence of $M_{rs}/M_s$ for members of the oxidized FA75 suite with oxidation temperature $T_{ox}$ as a parameter.

(Klapel & Shive 1975). A varying relative importance of $M_s$, $K$ and $\lambda$ with varying microstructure will therefore produce a varying temperature dependence of, for example, $H_c$.

The models for the magnetization process parameters apply to idealized microstructures (e.g. identical dispersed, randomly orientated ellipsoids of revolution with coherent magnetization reversal; or, for incoherently organized spin structures, a uniform fluctuation in surface or internal defects which is the same for all particles in the assemblage). In applying the models to the present data, parameters having the dimensions of length, or dimensionless parameters related to the shape of particles can be derived. While these have no simple interpretation they may indicate the origin of the microstructural variations in the present suite of samples.

### 4.2.1 *Monodomain models*

*4.2.1.1 Thermal fluctuation analysis—inferred grain volumes and elongations.* Considering first aligned particles with uniaxial anisotropy in the monodomain state, the coercive force is (e.g. Jacobs & Bean 1963).

$$H_c(T) = H^*(T) - T[2H^*(T)kT \ln (f_0 t^*)/\mu_0 M_s(T) v]^{1/2}$$

where $H^*(T)$ is the 'coercive force in the absence of thermal fluctuations', $k$ is Boltzmann's constant, $f_0$ is the frequency factor ($\simeq 10^{-10}\,s^{-1}$), $t^*$ is the characteristic time of measurement, $\mu_0 = 4\pi \times 10^{-7}\,Hm^{-1}$, and $v$ is the grain volume. $H_c$ is measured parallel to the grain axes. $H^*(T) = 2E_b(T)/\mu_0 M_s(T)$ where $E_b(T)$ is the height (per unit volume of particle) of the potential energy barrier to magnetization change. In the simplest case when shape anisotropy dominates, $E_b(T) = (\mu_0/2)(N_b - N_a)M_s^2(T)$ for ellipsoids of revolution with demagnetizing factors $N_b$ and $N_a$ in the unique plane and axis respectively. Following Dunlop's (1976) thermal fluctuation analysis the expression for $H_c(T)$ can then be rearranged so that

$$[H_c(T)/M_s(T)] = \Delta N - (\gamma\, \Delta N/v)^{1/2}[T^{1/2}/M_s(T)],$$

where $\Delta N$ replaces $(N_b - N_a)$ and $\gamma$ includes the constants. Fig. 6 shows the corresponding plot for three members of the FA75 suite $T_{ox} = 850\,°C$, $T_{ox} = 900\,°C$ and $T_{ox} = 1000\,°C$. To facilitate modelling the data, standard temperatures 0, 50, 100, 150 $\cdots$ 600 °C have been adopted and the $H_c$ values at each temperature interpolated from the measured values using the smooth curves of Fig. 4. The resulting

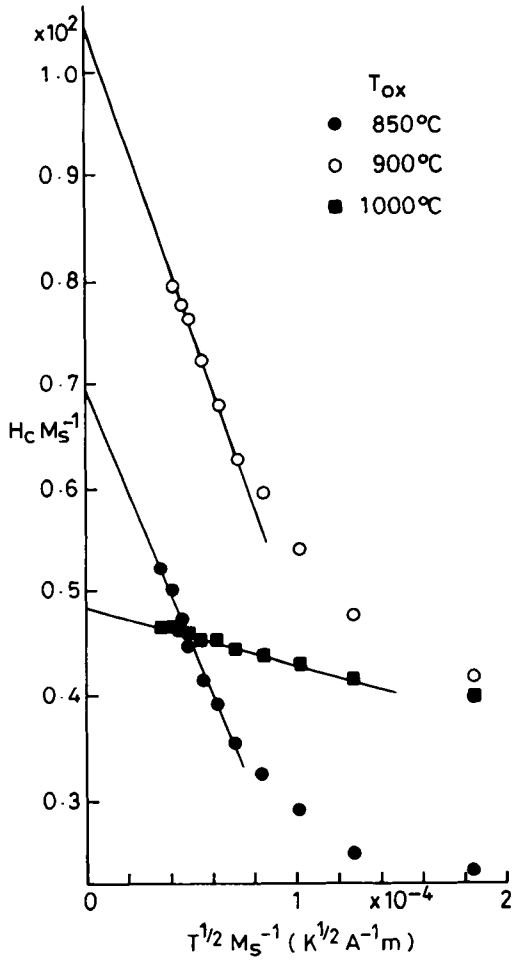


**Figure 6.** Selected plots of $H_c(T)/M_s(T)$ against $T^{1/2}/M_s(T)$ ('thermal fluctuation analysis'). The intercept gives a dimensionless parameter related to the elongation of model monodomain grains, and the intercept divided by the (slope)$^2$ multiplied by an appropriate numerical factor gives a parameter with the dimensions of volume. The derived parameters are listed in Table 2.

**Table 2.** Some measured and inferred properties of the magnetite produced by oxidation of FA75 at various oxidation temperatures ($T_{ox}$) under controlled atmosphere.

| $T_{ox}$ | $M_{rs}/M_s$ | $H_c$ (kA m$^{-1}$) | $L_{RT}$ ($\mu$m) | $\Delta N$ | $L_{HT}$ ($\mu$m) | $q$ | $N$ |
|---|---|---|---|---|---|---|---|
| 850 | 0.273 | 25.4 | | 0.07 | 0.05 | 3.2 | 0.15 |
| 900 | 0.408 | 35.8 | 0.1 | 0.09 | 0.07 | 2.5 | 0.20 |
| 950 | 0.380 | 37.2 | 0.1 | 0.09 | 0.1 | 2.2 | 0.23 |
| 1000 | 0.275 | 21.7 | 0.2 | 0.05 | 0.2 | 2.1 | 0.18 |
| 1060 | 0.18 | 15.3 | 0.3 | 0.04 | 1 | 2.0 | 0.17 |
| 1120 | 0.105 | 5.6 | 0.8 | — | — | 1.7 | — |

$L_{RT}$ is the *effective* grain size inferred from a comparison of room temperature $H_c$ with published data for magnetite grown crystals and crushed grains. $L_{HT}$ is the size inferred from thermal fluctuation analysis of the temperature dependence of $H_c$ (Figs 4 and 6). $\Delta N$ is a measure of the elongation of the grains by thermal fluctuation analyis (Figs 4 and 6). $q$ is the index parameter in the relation $H_c(T) \propto M_s^{q-1}(T)$ (Fig. 7). $N$ is the demagnetizing factor derived from the relation $M_{rs}(T) = H_c(T) \cdot N^{-1}$ (Fig. 8).

dimensionless intercepts are listed in Table 2. The values of $\Delta N$ would correspond to ellipsoids of revolution with $b/a = 0.6$–$0.8$. The ratio of intercept/(slope)$^2$ was multiplied by the factor $2k \ln (f_0 t^*)/\mu_0$ with $t^* = 1$ s, and the cube root taken to give a parameter with the dimension of length. These are also listed in Table 2. The method seems inapplicable to $T_{ox} = 1120$ °C (not shown) the plot having a positive slope. The straight lines are fitted to the $T_{ox} = 850$ °C and $T_{ox} = 900$ °C data (Fig. 6) for temperatures below 350 °C. The deviations from the straight lines suggest that $H_c$ above 350 °C is too high for the thermal fluctuation model. Similar, though much less pronounced trends may be discerned in the analysis of Dunlop & Bina (1977) (their Fig. 2).

In a recent adaption of the method, Dunlop, Özdemir & Enkin (1987) suggest substituting the measured initial susceptibility $\chi$ at elevated temperature for the hypothetical temperature variation of $H^*$. For randomly aligned grains with uniaxial symmetry $\chi(T) = \mu_0 M_s^2(T)/3E_b(T)$. Thus the analysis of Fig. 6 is performed by plotting $H_c(T)\chi(T)/M_s(T)$ against $T^{1/2}\chi^{1/2}(T)/M_s(T)$. Of course, when $E_b(T)$ results from shape anisotropy $\chi(T) =$ constant and the inclusion of $\chi$ in the analysis does not change the form of the thermal fluctuation plot. This is largely the case for the present data where Fig. 3 shows $\chi(T)$ varying significantly only near the Curie point. Taking $T_{ox} = 850$ °C, which has the greatest $\chi(T)$ variation, the modified thermal fluctuation plot (not shown) has an even greater divergence at high temperature from the low temperature linear trend. The more obvious defects of the model seem unlikely to account for this divergence. We suppose a non-aligned assemblage is accommodated by an $H^*(T)$ modified by a constant factor; the presence of fine particles with small enough $v$ so that $H_c(T) = 0$ at higher temperatures would reduce the measured $H_c$; particle–particle interactions, which are difficult to model, might be expected to have the same temperature dependence as shape anisotropy, both being essentially the same magnetostatic phenomenon. It may be that the divergence is caused not by what may be relatively minor differences, given suitable experimental material, but by a gross inapplicability of the model, e.g. thermal fluctuations only being important very close to $T_c$, or that grains contain domains.

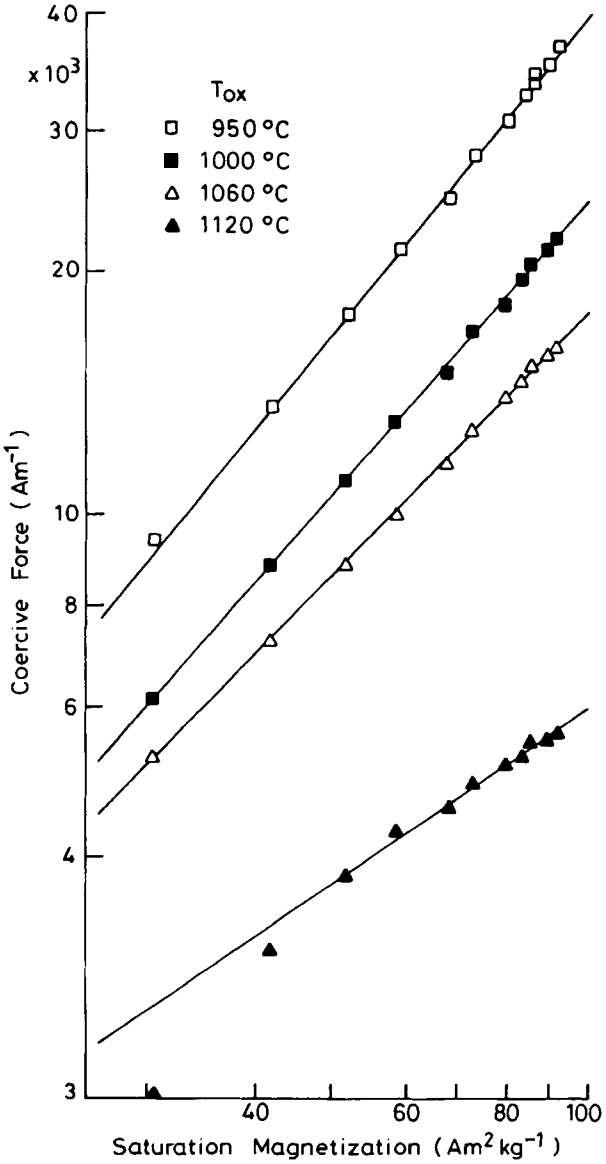


**Figure 7.** Selected plots of $\log H_c$ against $\log \sigma_s$ ($\sigma_s$ is the magnetization per unit mass). The slopes of the plots are equated to $(q - 1)$ and the parameter $q$ is listed in Table 2.

*4.2.1.2 The monodomain model without thermal fluctuations—effect of particle interactions*? If thermal fluctuations are not important and the particles are monodomain then $H_c(T) = H^*(T) \propto E_b(T)/M_s(T)$. For shape anisotropy $E_b(T) \propto M_s^2(T)$, for strain anisotropy $E_b(T) \propto \lambda(T)$ and crystal anisotropy $E_b(T) \propto K_1(T)$. When $\lambda(T)$ and $K_1(T)$ can be expressed as simple power law, $M_s^q(T)$, the slope of the $\log H_c(T) - \log M_s(T)$ plots have slope $q - 1$. Some representative plots are shown in Fig. 7. Straight lines give plausible fits to the data and the derived values of $q$ are listed in Table 2. The values lie near the $q = 2$ expected from strain or shape anisotropy, although the lower $T_{ox}$ are significantly higher, and a systematic variation of $q$ with $T_{ox}$ is observed.

An explanation for the increase in $q$ in the lower $T_{ox}$ samples may lie in competing anisotropies of cubic (magnetocrystalline, $q \sim 8$) and uniaxial (shape or strain,

$q \sim 2$) symmetries. The dipole–dipole interaction energy also has a uniaxial symmetry and an $M^2$ dependence. Two ellipsoidal grains, broadside on to each other at distance $l$, have a potential energy $(\mu_0\mu^2/4\pi) \cdot [3(N_b - N_a)/2r^3 - 3/l^3] \sin^2\theta$, where $\mu$ is the grain moment, $r$ the grain size and $\theta$ the angle between the moments and the grain axes. The factor 3 in the $3/l^3$ dipolar term applies to rotation in unison and will be reduced to 0.25 when the moments rotate by 'fanning' (and, of course, for particles in line astern the two bracketed terms will no longer oppose each other but *add* together). The two terms can conceivably be of comparable size, so that with a suitably contrived microstructure (predominantly 'broadside-on') the uniaxial term can become small compared to a co-existing cubic term. The effect of the competing cubic and uniaxial terms on the coercive force depends on the orientation of the axes of the two symmetries (see, e.g. Özdemir & O'Reilly 1981). $H_c$ may be raised or lowered compared to that resulting from (say) the uniaxial symmetry alone. Here we are concerned with the temperature dependence of $H_c$. This would be determined by the relative contributions of the two symmetries rather than whether they collaborated or opposed.

It may be possible therefore to construct a plausible microstructural model in which the interplay of the three factors—the co-existing cubic and uniaxial anisotropies within the grains and the intergrain interactions—varies with $T_{ox}$. In the lower $T_{ox}$ dendritic material, the uniaxial and interaction terms compete and allow the cubic symmetry to become visible in a $q$ value in excess of 2. As $T_{ox}$ rises, and the structure becomes less dendritic and more symplectite-like, the interaction term is less effective in reducing the uniaxial term which then dominates over the cubic so that $q$ approaches the value 2.

### 4.2. *Multidomain models*

*4.2.2.1 Inferences about domain wall pinning.* The coercive force for a two-domain model grain is $H_c = (\Delta E_w)k/2\mu_0 M_s$ where $\Delta E_w$ is the amplitude and $k$ the wave number of the wall energy (per unit area) fluctuation. Stacey & Wise (1967) proposed that $(\Delta E_w)$ would depend on the particle dimension $L$ if the number of crystal defects within the volume of the domain wall fluctuated randomly as the wall translated through the particle. Thus $(\Delta E_w)_v$, the fluctuation in $E_w$ arising from the volume of the wall, $\propto L^{-1}$. If the wall may also be pinned by surface defects, then the average number of defects at the surface intersected by the wall is of the order $\nu L\,\delta$, where $\nu$ is the average number of defects per unit area, $L$ is the dimension of the rectangular grain and $\delta$ the wall thickness. The fluctuation in the average number of surface defects sampled by the wall is $(\nu L\,\delta)^{1/2}$. The corresponding fluctuation in total wall energy is $(\Delta E_w)_s L^2$, so that $(\Delta E_w)_s \propto L^{-3/2}$. The total wall energy fluctuation due to the two uncorrelated fluctuations is $(\Delta E_w) = [(\Delta E_w)^2 + (\Delta E_w)_s^2]^{1/2}$. Such an expression has been used to fit the particle size dependence of room temperature $H_c$ for titanomagnetites (O'Donovan, Facey & O'Reilly 1986). Here we are concerned with the temperature dependence. As before, the barriers to magnetization change $(\Delta E_w)$ depend on $K$ and $\lambda$, so that if $(\Delta E_w) \propto M_s^q(T)$, $H_c \propto M_s^{q-1}(T)$. The problem again is to find reasons why $K$ and $\lambda$ should make contributions which vary with $T_{ox}$. A possibility is that the two material properties make different contributions to $(\Delta E_w)_v$ and $(\Delta E_w)_s$. $(\Delta E_w)_s$ will become relatively more important with respect to $(\Delta E_w)_v$ as $L$ decreases. The higher values of $q$ for low $T_{ox}$ in Table 2 would then require that $K$ plays a more important role in the surface pinning of domain walls than in volume pinning.

*4.2.2.2 Inferences about the demagnetizing factor.* The two-domain model grain has a sheared rectangular hysteresis loop, the slope of the ascending and descending sides being $N^{-1}$ so that $M_{rs} = H_c/N$. The demagnetizing factor $N$ is well defined only in homogeneously magnetized ellipsoids. For a two-domain cube, Dunlop (1983) has shown that the effective demagnetizing factor varies with the position of the wall by about 20 per cent and is approximately 1/6. $N$ may be evaluated by plotting $M_{rs}(T)$ against $H_c(T)$. This process may also reveal increases in domain multiplicity as temperature rises. The $M_{rs}$ versus $H_c$ plots for the FA75 series derived from the data of Figs 4 and 5 are shown in Fig. 8. The corresponding values of $N$, which are listed in Table 2, lie between the model two-domain cube ($N = 0.13$) and the many-domain sphere ($N = 0.33$). The first three samples, $T_{ox} = 850$, 900 and 950 °C, suggest a trend of increasing domain multiplicity with increasing $T_{ox}$ but this breaks down when $T_{ox} = 1000$ °C and above, for which $M_{rs}(T)$ is either too high or $H_c(T)$ too low. The change in slope of the $T_{ox} = 950$ and 1000 °C plots are consistent with an increase in $N$ (suggesting an increase in number of domains) as $T$ rises. The $T_{ox} = 1120$ °C sample (not shown) has $N = 0.08$ (below 350 °C) and $N = 0.14$ (above 400 °C). An alternative route to evaluating $N$, using Hodych's (1986) relation

$$\chi(T)^{-1} = k^{-1}H_c(T)/M_s(T) + N$$

failed to give acceptable linear fits with the data of the present samples.

## 5 CONCLUSIONS

The deuteric oxidation of natural olivine has been simulated in the laboratory by heating synthetic Fe–Mg olivines at temperatures between 850 and 1280 °C under controlled atmospheres produced by $CO$–$CO_2$ mixtures. The magnetic constituent of the resultant intergrowths is magnetite, $Fe_3O_4$, in concentrations up to about 20 per cent. The simulation successfully produced both the 'dendritic' intergrowths and 'symplectite' intergrowths which are found in nature, the former at temperatures below about 1150 °C and the latter at higher temperatures.

The microstructure-dependent magnetization process parameters of the produced magnetite correlate with the oxidation temperature. Although the dendritic intergrowths are too complex to be easily reduced to one or two microstructural parameters such as 'particle size' and 'length/diameter ratio', such parameters can be derived from the magnetization process data either by comparison with data on simpler well-characterized material, or by fitting the data to physical models for the temperature

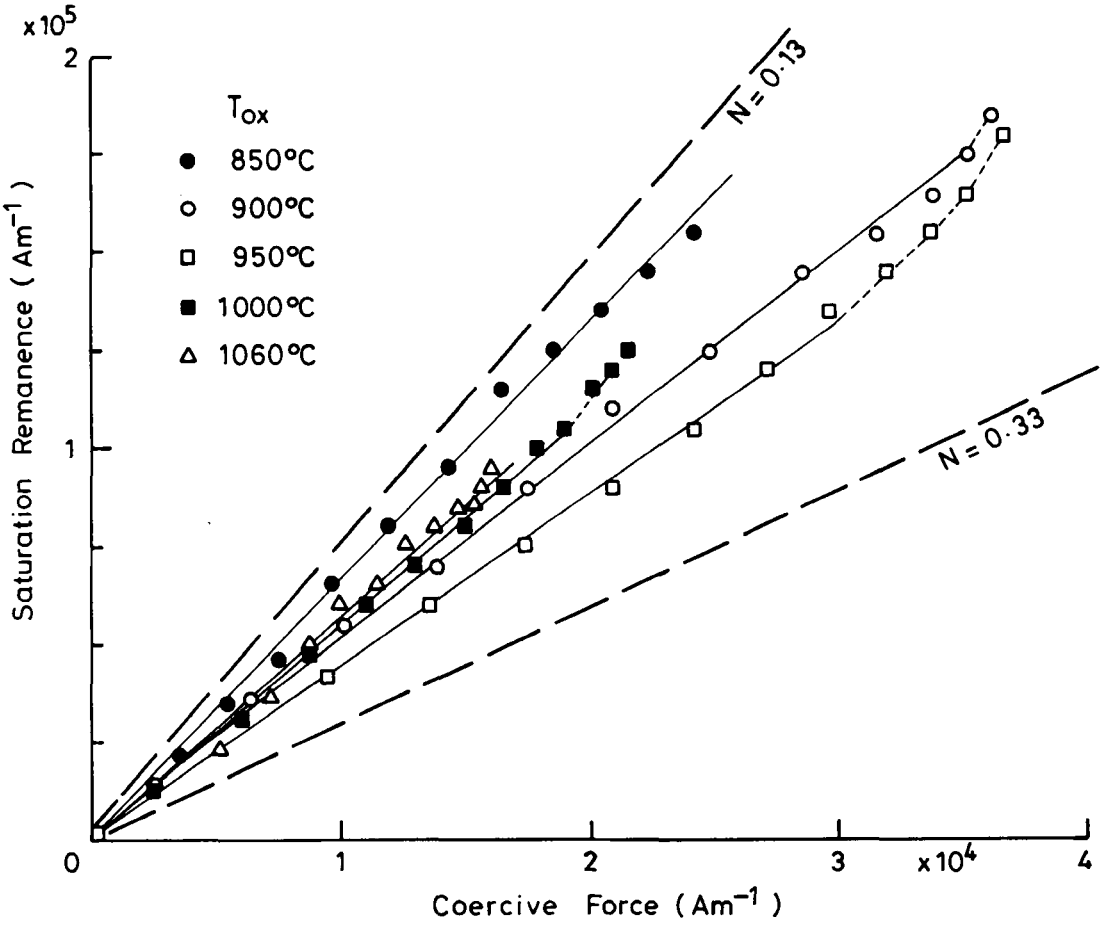


**Figure 8.** Saturation remanence $M_{rs}(T)$ plotted against $H_c(T)$ with $T_{ox}$ as a parameter. The slopes of the lines are equated to $N^{-1}$, and the values of $N$ are listed in Table 2.

dependence of the magnetization process which contain microstructural parameters. The comparison with published data for material of measured particle size suggests the magnetite in the present suite of oxidized olivine has *effective* grain size increasing from about 0.1 to about 3 $\mu$m as the oxidation temperature rises from 900 to 1200 °C. The produced magnetite is 'hard' and could be expected to acquire an intense and stable thermoremanence.

The measured magnetization process parameters suggest that the intergrowths behave like particles with one or a few domains. Application of the model expression for the temperature dependence of the coercive force in monodomain grains subject to thermal agitation yields plausible grain dimensions and length/diameter ratios, the higher oxidation temperature producing larger, more equidimensional particles. The application of an alternative model, in which the grains are not subject to thermal fluctuations and which does not explicitly involve microstructural parameters, nevertheless points to the relation between the oxidation temperature and the resultant microstructure. In this case a plausible qualitative description of the results of the analysis lies in the competition between anisotropies of different symmetries—one cubic and the other uniaxial—the uniaxial term being influenced by the interparticle field in dendritic intergrowths.

Models for grains which contain domains may also be applied to the temperature variations of magnetization process parameters. If domain walls are pinned by both surface and volume defects, a decreasing relative proportion of surface to volume with increasing oxidation temperature may be suggested by the application of the model. Plausible values of demagnetizing factor, appropriate to grains with few domains are produced by the model.

Finally, which give the better fits to the data—the monodomain or multidomain models? The answer is probably 'neither'. This may be an expression of the fact there is no evidence even in simpler materials that experimentally the magnetization process characteristics can be divided into two such regimes. Nor is it clear that the models actually predict a change as the number of domains goes from 1 to 2 which is more dramatic than from 2 to 3 and so on.

## ACKNOWLEDGMENTS

This investigation forms part of an NERC sponsored investigation: The magnetic mineralogy of igneous rocks studied by magnetic methods: the chemical basis of palaeomagnetism. One of the authors (DB) has been in receipt of an NERC studentship. We also thank Dr J. B. O'Donovan for invaluable assistance in the preparation of materials.

## REFERENCES


Bowen, N. L. & Schairer, J. F., 1935. The system MgO–FeO–SiO, *Am. J. Sci.*, **229,** 151–217.

Brearley, A. J. & Champness, P. E., 1986. Magnetite exsolution in alamandine garnet, *Mineral. Mag.*, **50,** 621–633.

Champness, P. E. & Gay, P., 1968. Oxidation of olivines, *Nature*, **218,** 157–158.

Davis, K. E., 1981. Magnetite rods in plagioclase as the primary carrier of stable NRM in ocean floor gabbros, *Earth planet. Sci. Lett.*, **55,** 190–198.

Dunlop, D. J., 1976. Thermal fluctuation analysis, a new technique in rock magnetism, *J. geophys. Res.*, **81,** 3511–3617.

Dunlop, D. J., 1983. On the demagnetizing energy and demagnetizing factor of a multidomain ferromagnetic cube, *Geophys. Res. Lett.*, **10,** 79–82.

Dunlop, D. J., 1986. Hysteresis properties of magnetite and their dependence on particle size: a test of pseudo-single domain remanence models, *J. geophys. Res.*, **91,** 9569–9584.

Dunlop, D. J. & Bina, M.-M., 1977. The coercive force spectrum of magnetite at high temperatures: evidence for thermal activation below the blocking temperature. *Geophys. J. R. astr. Soc.*, **51,** 121–147.

Dunlop, D. J., Özdemir, Ö. & Enkin, R. J., 1987. Multidomain and single-domain relations between susceptibility and coercive force, *Phys. Earth planet. Int.*, **49,** 181–191.

Evans, M. E., McElhinny, M. W. & Gifford, A. C., 1968. Single domain magnetite and high coercivities in a gabbroic intrusion, *Earth Planet. Sci. Lett.*, **9,** 142–146.

Fletcher, E. J. & O'Reilly, W., 1974. Contribution of $Fe^{2+}$ ions to the magnetocrystalline anisotropy constant $K_1$ of $Fe_{3-x}Ti_xO_4$ ($0 < x < 0.1$), *J. Phys. C.*, **7,** 171–178.

Haggerty, S. E. & Baker, I., 1967. The alteration of olivine in basaltic and associated lavas. Part I: High temperature alteration, *Contrib. Miner. Petrol.*, **16,** 233–257.

Hargraves, R. B. & Young, W. M., 1969. Source of stable remanent magnetism in Lambertville diabase, *Am. J. Sci.*, **267,** 1161–1177.

Hodych, J. P., 1986. Determination of self-demagnetizing factor N for multidomain grains in rocks, *Phys. Earth planet. Int.*, **41,** 283–291.

Hoffmann, V. & Soffel, H. C., 1986. Magnetic properties and oxidation experiments with synthetic olivines $(Fe_xMg_{1-x})_2SiO_4$, $0 < x < 1$. *J. Geophys.*, **60,** 41–46.

Hoye, G. S. & Evans, M. E., 1975. Remanent magnetizations in oxidized olivines, *Geophys. J. R. astr. Soc.*, **41,** 139–151.

Hoye, G. S. & O'Reilly, W., 1972. A magnetic study of the ferromagnesian olivines $(Fe_xMg_{1-x})_2SiO_4$, $0 < x < 1$, *J. Phys. Chem. Solids*, **33,** 1827–1834.

Hoye, G. S. & O'Reilly, W., 1973. Low temperature oxidation of ferromagnesian olivines—a gravimetric and magnetic study, *Geophys. J. R. astr. Soc.*, **33,** 81–92.

Jacobs, I. S. & Bean, C. P., 1963. Fine particles, thin films and exchange anisotropy (effects of finite dimensions and interfaces on the basic properties of ferromagnets), in *Magnetism*, pp. 271–350, ed. Rado, G. T. & Suhl, H., Academic Press, New York.

Klapel, G. D. & Shive, P. N., 1975. High temperature magnetostriction of magnetite, *J. geophys. Res.*, **79,** 2629–2633.

Lindsley, D. H., 1976. Experimental studies of oxide minerals, In *Oxide Minerals*, chap. 2, ed. Rumble, D. III, Mineralogical Society of America, Washington.

Morgan, G. E. & Smith, P. P. K., 1981. Transmission electron microscope and rock magnetic investigations of remanence carriers in a Pre-Cambrian metadolerite, *Earth planet. Sci. Lett.*, **53,** 226–240.

Nitsan, U., 1974. Stability field of olivine with respect to oxidation and reduction, *J. geophys. Res.*, **79,** 706–711.

O'Donovan, J. B., Facey, D. & O'Reilly, W., 1986. The magnetization process in titanomagnetite ($Fe_{2.4}Ti_{0.6}O_4$) in the 1–30 $\mu$m particle size range. *Geophys. J. R. astr. Soc.*, **87,** 897–916.

Putnis, A., 1979. Electron petrography of high temperature oxidation in olivine from the Rhum layered intrusion, *Miner. Mag.*, **43,** 293–296.

Riding, A., 1969. Magnetic materials in oxidized olivine and their contribution to the natural remanent magnetization of rocks. The natural remanent magnetization of some Triassic red sandstone, *PhD thesis*, University of Liverpool.

Stacey, F. D. & Wise, K. N., 1967. Crystal dislocations and coercivity of fine grained magnetite, *Aust. J. Phys.*, **20,** 507–513.